Open access • Journal Article • DOI:10.1088/0004-637X/784/1/85

# Constraints on Shallow 56Ni from the Early Lightcurves of Type Ia Supernovae



Anthony L. Piro, Ehud Nakar

**Institutions:** California Institute of Technology, Tel Aviv University

**Published on:** 27 Nov 2012 - arXiv: High Energy Astrophysical Phenomena

**Topics:** Supernova and White dwarf

The Astrophysical Journal, 784:85 (9pp), 2014 March 20 doi:10.1088/0004-637X/784/1/85


# CONSTRAINTS ON SHALLOW $^{56}$Ni FROM THE EARLY LIGHT CURVES OF TYPE Ia SUPERNOVAE

Anthony L. Piro[1] and Ehud Nakar[2]
[1] Theoretical Astrophysics, California Institute of Technology, 1200 E California Boulevard, M/C 350-17, Pasadena, CA 91125, USA; piro@caltech.edu
[2] Raymond and Beverly Sackler School of Physics and Astronomy, Tel Aviv University, Tel Aviv 69978, Israel
*Received 2012 November 26; accepted 2014 February 13; published 2014 March 6*

## ABSTRACT

Ongoing transient surveys are presenting an unprecedented account of the rising light curves of Type Ia supernovae (SNe Ia). This early emission probes the shallowest layers of the exploding white dwarf (WD), which can provide constraints on the progenitor star and the properties of the explosive burning. We use semianalytic models of radioactively powered rising light curves to analyze these observations. As we have summarized in previous work, the main limiting factor in determining the surface distribution of $^{56}$Ni is the lack of an unambiguously identified time of explosion, as would be provided by detection of shock breakout or shock-heated cooling. Without this the SN may in principle exhibit a "dark phase" for a few hours to days, where the only emission is from shock-heated cooling that is too dim to be detected. We show that by assuming a theoretically motivated time-dependent velocity evolution, the explosion time can be better constrained, albeit with potential systematic uncertainties. This technique is used to infer the surface $^{56}$Ni distributions of three recent SNe Ia that were caught especially early in their rise. In all three we find fairly similar $^{56}$Ni distributions. Observations of SN 2011fe and SN 2012cg probe shallower depths than SN 2009ig, and in these two cases $^{56}$Ni is present merely $\sim 10^{-2}$ $M_{\odot}$ from the WDs' surfaces. The uncertainty in this result is up to an order of magnitude given the difficulty of precisely constraining the explosion time. We also use our conclusions about the explosion times to reassess radius constraints for the progenitor of SN 2011fe, as well as discuss the roughly $t^2$ power law that is inferred for many observed rising light curves.

*Key words:* hydrodynamics – shock waves – supernovae: general – white dwarfs

## 1. INTRODUCTION

Type Ia supernovae (SNe Ia) play a central role in modern astrophysics. They are used as distance indicators to probe the expansion of the universe (Riess et al. 1998; Perlmutter et al. 1999), they produce most of the iron-group elements in the cosmos (Iwamoto et al. 1999), and they provide an astrophysical context for studying explosions (Hillebrandt & Niemeyer 2000). But their importance has brought attention to the theoretical uncertainties that frustratingly remain. It is generally accepted that they result from unstable thermonuclear ignition of degenerate matter (Hoyle & Fowler 1960) in a C/O white dwarf (WD), but the progenitor systems have not been identified. Candidates include stable accretion from a non-degenerate binary companion (Whelan & Iben 1973), the merging of two C/O WDs (Iben & Tutukov 1984; Webbink 1984), or accretion and detonation of a helium shell on a C/O WD that leads to core detonation (Woosley & Weaver 1994a; Livne & Arnett 1995). In addition, it is not known whether the incineration proceeds as a sub-sonic deflagration (Nomoto et al. 1976, 1984) or deflagration-detonation transition (DDT; Khokhlov 1991; Woosley & Weaver 1994b). Each scenario has implications for the velocity profile, density structure, and distribution of ashes within the exploding WD.

A powerful method for constraining between these models is the study of the early-time behavior of SNe Ia, since this is when the shallowest layers of the WD are probed by the observed emission. Analysis of spectra provides one way of learning about the surface abundances of these explosions (e.g., Hachinger et al. 2013). The photometry is also sensitive to the depth and distribution of radioactive heating (Piro 2012; Piro & Nakar 2013). With early observations of SNe Ia becoming more common, the time is ripe to explore what can be learned from these measurements.

In the following work we use semianalytic models to study where and how much $^{56}$Ni is present in the outer ejecta of SNe Ia. As discussed in our previous investigation of radioactively powered light curves (Piro & Nakar 2013), it is difficult to directly measure the $^{56}$Ni distribution without a detection of the explosion time, as would be provided by shock breakout or shock-heated cooling (Piro et al. 2010; Nakar & Sari 2010, 2012; Rabinak et al. 2012). Unfortunately, in the case of SNe Ia, such emission has never been detected because of the small WD radius. If merely photometric light curves of the rise are available, there is a degeneracy between emission being from $^{56}$Ni near the surface with a recent explosion versus $^{56}$Ni deeper in the star but with an explosion further in the past. In the latter case, an SN Ia exhibits a "dark phase" for a few hours to days until the thermal diffusion wave reaches the shallowest $^{56}$Ni deposits. Even with these uncertainties, constraints can still be provided by comparing a wider range of properties, such as the velocity evolution. This information is available for a few well-studied SNe Ia, and we use it in order to estimate the time of explosion and surface $^{56}$Ni distribution for each of them.

In Section 2 we summarize the semianalytic framework used to model the rising light curves. In Section 3 we analyze observations of three recent SNe Ia and summarize our constraints on their shallow $^{56}$Ni distributions. In Section 4 we consider the $t^2$ rise that is often observed in early light curves and discuss whether $t^2$ (or any power law) should be expected. We conclude in Section 5 with a summary of our results and a discussion of future work.

## 2. RADIOACTIVELY POWERED RISING LIGHT CURVES

In the following we present the model used for this study, which borrows from and builds upon our recent work on

radioactively powered rising light curves. In Piro (2012), we focused on direct $^{56}$Ni heating at the depth of the diffusion wave. In Piro & Nakar (2013), we added the "diffusive tail," which provides heating at depths shallower than the intrinsic $^{56}$Ni distribution. Here we include these effects in greater detail by integrating over their contributions throughout the WD, as discussed in Appendix B of Piro & Nakar (2013). We quickly summarize the main results here for completeness.

As the ejecta from the SN expands, a thermal diffusion wave travels back through the material. This is defined as the depth at which photons can diffuse up to the surface of the exploding star within the time since the start of the explosion. This condition is satisfied where the optical depth to the observer is approximately $c/v$, where $c$ is the speed of light and $v$ is the velocity of the expanding gas at the location of the diffusion wave. Note that the diffusion depth (at optical depth greater than unity) is considerably deeper than the photosphere. At any time $t$, the diffusion wave has a depth of roughly

$$\Delta M_{\rm diff} \approx 2\times10^{-2}\frac{E_{51}^{0.44}}{\kappa_{0.1}^{0.88}M_{1.4}^{0.32}}\left(\frac{t}{1\,{\rm day}}\right)^{1.76}M_{\odot}, \quad (1)$$

where $E = 10^{51}E_{51}$ erg is the explosion energy, $M = 1.4\,M_{1.4}\,M_{\odot}$ is the ejecta mass, and $\kappa = 0.1\kappa_{0.1}$ cm$^2$ g$^{-1}$ is the opacity. We approximate the opacity as constant. This is motivated by the fact that during the times at which we are modeling these events the bolometric luminosity is always greater than $10^{41}$ erg s$^{-1}$. Combined with the times of explosion that we derive, along with the observed photospheric velocities, we infer that the temperature at the diffusion depth is always $>10{,}000$ K during the rising phase. Thus, carbon and oxygen are always ionized at least once, and if these elements dominate the opacity then it is in the range 0.03–0.2 cm$^2$ g$^{-1}$. If the outer layers have sufficient $^{56}$Ni to dominate the opacity, then it is $\sim$0.1 cm$^2$ g$^{-1}$ (Pinto & Eastman 2000). Therefore, our opacity assumption introduces at most a factor of three error in the diffusion depth. The scalings and prefactors in Equation (1) use Appendix C of Piro & Nakar (2013) with values appropriate for Chandrasekhar mass WDs.

At the times we consider, the ejecta is optically thick to gamma-rays emitted from radioactive decay, and they efficiently heat the SN. Heating in material shallower than $\Delta M_{\rm diff}$ directly goes into the observed luminosity. Heating in material deeper than $\Delta M_{\rm diff}$ only contributes to the observed light curve if some fraction of the photons from these larger depths are able to diffuse up to $\Delta M_{\rm diff}$. This produces the so-called diffusive tail. Motivated by this picture, we split the total observed luminosity into two parts

$$L(t) = L_{\rm direct}(t) + L_{\rm tail}(t), \quad (2)$$

where $L_{\rm direct}$ is the direct heating by $^{56}$Ni down to $\Delta M_{\rm diff}$, and $L_{\rm tail}$ is the diffusive tail from material deeper than $\Delta M_{\rm diff}$. Each is an integral over different regions of the ejecta. For the direct heating component

$$L_{\rm direct}(t) = \int_0^t X_{56}(t')\frac{\partial\Delta M_{\rm diff}}{\partial t'}\epsilon(t)dt', \quad (3)$$

where $X_{56}(t)$ is the mass fraction of $^{56}$Ni at the depth of the diffusion wave at time $t$, and the specific heating rate is

$$\epsilon(t) = \epsilon_{\rm Ni}e^{-t/t_{\rm Ni}} + \epsilon_{\rm Co}(e^{-t/t_{\rm Co}} - e^{-t/t_{\rm Ni}}), \quad (4)$$

where $\epsilon_{\rm Ni} = 3.9\times10^{10}$ erg g$^{-1}$ s$^{-1}$, $t_{\rm Ni} = 8.76$ days, $\epsilon_{\rm Co} = 7.0\times10^{9}$ erg g$^{-1}$ s$^{-1}$, and $t_{\rm Co} = 111.5$ days. The total diffusive tail component is the integral over all the diffusive tails from heating deeper than $\Delta M_{\rm diff}$,

$$L_{\rm tail}(t) = \int_t^{t_{\rm diff}} X_{56}(t')\frac{\partial\Delta M_{\rm diff}}{\partial t'}\epsilon(t)\frac{{\rm erfc}(t'/\sqrt{2}t)}{{\rm erfc}(1/\sqrt{2})}dt'. \quad (5)$$

We take the upper integration limit to be the diffusion time through the entire ejecta $t_{\rm diff}$,[3] which roughly corresponds to the time of light curve peak.

Since $\Delta M_{\rm diff} \propto t^{1.76}$, Equations (3) and (5) are rewritten as

$$L_{\rm direct}(t) = 1.76L_{56}(t)\int_0^t \frac{X_{56}(t')}{X_{56}(t)}\left(\frac{t'}{t}\right)^{1.76}\frac{dt'}{t'}, \quad (6)$$

and

$$L_{\rm tail}(t) = 1.76L_{56}(t)\int_t^{t_{\rm diff}} \frac{X_{56}(t')}{X_{56}(t)}\left(\frac{t'}{t}\right)^{1.76}\frac{{\rm erfc}(t'/\sqrt{2}t)}{{\rm erfc}(1/\sqrt{2})}\frac{dt'}{t'}, \quad (7)$$

where

$$L_{56}(t) \equiv X_{56}(t)\Delta M_{\rm diff}(t)\epsilon(t) \quad (8)$$

is roughly the local heating rate from $^{56}$Ni. The luminosity has no contribution from the diffusive tail once the diffusion wave has traveled through the ejecta, thus we define $L_{\rm diff} \equiv L_{\rm direct}(t = t_{\rm diff})$.

When actually performing calculations, it is useful to write these expressions in dimensionless forms. First, let $x \equiv t/t_{\rm diff}$ and $x' \equiv t'/t_{\rm diff}$, where $x$ and $x'$ vary from 0 to 1. We define the ratio of the local heating rate to $L_{\rm diff}$ as

$$\Lambda(x) \equiv 1.76\frac{L_{56}(x)}{L_{\rm diff}} = \frac{\epsilon(x)}{\epsilon(1)}\left[\int_0^1 \frac{X_{56}(x')}{X_{56}(x)}\left(\frac{x'}{x}\right)^{1.76}\frac{dx'}{x'}\right]^{-1}. \quad (9)$$

The ratio of the observed time-dependent luminosity to $L_{\rm diff}$ is then

$$\frac{L(x)}{L_{\rm diff}} = \Lambda(x)\int_0^x \frac{X_{56}(x')}{X_{56}(x)}\left(\frac{x'}{x}\right)^{1.76}\frac{dx'}{x'} + \Lambda(x)\int_x^1 \frac{X_{56}(x')}{X_{56}(x)}\left(\frac{x'}{x}\right)^{1.76}\frac{{\rm erfc}(x'/\sqrt{2}x)}{{\rm erfc}(1/\sqrt{2})}\frac{dx'}{x'}. \quad (10)$$

In this form the right-hand side is dimensionless and only depends on the $^{56}$Ni distribution. This allows us to vary $X_{56}(x)$ and calculate a wide range of light curves, which can then be rescaled to a particular observation via $L_{\rm diff}$ and $t_{\rm diff}$.

When fitting a $^{56}$Ni distribution to a given light curve in the next section, we use the parameterization

$$X_{56}(x) = \frac{X'_{56}}{1+\exp[-\beta(x-x_{1/2})]}, \quad (11)$$

[3] Note that in this work we are using a different definition of $t_{\rm diff}$ than that in Piro & Nakar (2013).

where $X'_{56}$ sets the normalization, $\beta$ controls the steepness of the rise, and $x_{1/2}$ is the time when $X_{56}/X'_{56} = 1/2$. This allows us to consider a variety of $^{56}$Ni distributions with two parameters. The normalization is determined by

$$X'_{56} = \frac{L_{\rm diff}}{1.76\Delta M_{\rm diff}(t_{\rm diff})\epsilon(t_{\rm diff})} \times \left[\int_0^1 \frac{x'^{0.76}dx'}{1+\exp[-\beta(x'-x_{1/2})]}\right]^{-1}, \quad (12)$$

and thus is not a free parameter. The drawback of this parameterization is that we can only consider $^{56}$Ni distributions that increase with depth. A more complicated distribution is a realistic possibility, such as in a double detonation where there may be a surface enhancement of $^{56}$Ni from explosive burning of a helium shell (Shen & Bildsten 2009; Fink et al. 2010). In future studies we will better explore such $^{56}$Ni distributions.

## 3. COMPARISONS TO SPECIFIC SUPERNOVAE

Recent observations have been especially fruitful in catching SNe Ia at early times. We use this work to analyze three well-studied events: SN 2011fe, SN 2012cg, and SN 2009ig. For each we summarize what can be constrained from their photometric light curves and velocity evolution. Although there are particular issues for each event (which we discuss below), our general strategy is as follows.

1. Since an SN may in principle exhibit a dark phase, we assume that the time of explosion is not known.
2. For a spectral line generated at constant specific opacity, its velocity is a power law with time with $v \propto t^{-0.22}$ (Piro & Nakar 2013). We vary the explosion time and check when the observed absorption features best match this power law. From this we infer what is the likely explosion time.
3. The photospheric velocity $v_{\rm ph}$ is expected to roughly follow the low-velocity Si II $\lambda$6355 absorption feature (Tanaka et al. 2008). Using the fits performed in the previous step, we can therefore estimate $v_{\rm ph}(t)$. The photospheric radius is then given by $r_{\rm ph} = v_{\rm ph}t$.
4. Assuming that the SN emits roughly as a blackbody and using the observed $B$, $V$, and $R$ light curves, we fit the color temperature $T_c$ and bolometric luminosity as a function of time using $L \approx 4\pi r_{\rm ph}^2 \sigma_{\rm SB} T_c^4$. Using just these wave bands, the inferred bolometric luminosity is always a lower limit.
5. Theoretical light curves are generated with different $X_{56}(x)$ via Equation (10), where $X_{56}(x)$ has the functional form of Equation (11). We estimate $L_{\rm diff}$ and $t_{\rm diff}$ as roughly the peak luminosity and time of peak luminosity, respectively. In this way the theoretical light curves are rescaled for comparison with the bolometric light curve, and we can put constraints on what is the most likely distribution of $^{56}$Ni.

The largest limitation of this framework is our assumption of a specific time-dependent power law for the velocity evolution of $v \propto t^{-0.22}$ in step 2 above. As we show below, we find that all three of the absorption features we focus on roughly obey this same power-law dependence.[4] This would not have been the case if the method we use is entirely wrong, and thus this lends some support for our approach. Nevertheless, it is possible that small variations from the theoretically predicted power law introduce systematic errors. We try to better quantify the errors introduced by this fundamental assumption of our model by varying the exponent of the power law from 0.20 to 0.24 (see the discussions in the following sections). This shows that it is difficult to constrain the explosion time to better than roughly $\pm$0.5 day. Later this rough error is also used to quantify the uncertainty in the derived $^{56}$Ni distributions. Beyond this, it is difficult for us to further quantify how much different the $^{56}$Ni distribution could be if, for example, the photosphere evolved in a much more complicated way. A useful exercise would therefore be to use detailed numerical modeling from explosion simulations to better test these assumptions.

### 3.1. Modeling SN 2011fe

We first focus on SN 2011fe because it is the most constrained by our modeling. SN 2011fe exploded in 2011 August as the closest SNe Ia in the last 25 years (Nugent et al. 2011). The considerable interest in this event and its proximity make it one of the best studied SNe Ia. The time-dependent velocities of absorption features are summarized in Parrent et al. (2012). The $B$, $V$, and $R$ rising light curves are presented in Vinkó et al. (2012). This particular work was chosen because of the high density of observations during the rise, but we could have just as well considered other data sets (Richmond & Smith 2012; Munari et al. 2013). We use a distance modulus for M101 of 29.05 (Shappee & Stanek 2011), and no reddening is included because it has been inferred to be relatively small (Patat et al. 2013). The various studies have found different times for the peak bolometric luminosity, depending on the fitting method used. For the present work we choose a time of peak of JD2455815.4, although this choice does not greatly impact our conclusions for the $^{56}$Ni distribution at shallow depths. The earliest detection was at JD2455797.65 (Nugent et al. 2011), and their fitting of a $t^2$ power law to the rising luminosity (as is common practice) gives an explosion time of JD2455797.2 before the peak. Although they quote an error of $\pm$0.01 day, as we discuss later this practice is not well justified and the true uncertainty in the explosion time is considerably larger. Nugent et al. (2011) also observed the location of SN 2011fe roughly at JD2455796.7, which provides an upper limit in the apparent $g$-band magnitude of 21.5 (absolute magnitude of $-7.55$).

In our analysis of the velocity evolution, we use the low-velocity Si II $\lambda$6355, high-velocity Si II $\lambda$6355, and high-velocity Ca II H and K absorption features.[5] The velocities of the absorption lines are always calculated from the location of deepest absorption. In the top panel of Figure 1 we plot the $\chi^2$ found by fitting these features with power-law velocity profiles as a function of the explosion time, where $\chi^2$ is defined as

$$\chi^2 = \sum_N \left(\frac{v_N - v(t)}{\Delta v}\right)^2, \quad (13)$$

where $N$ is the number of data points, $v_N$ is a measured velocity, and $\Delta v = 500$ km s$^{-1}$ is a rough estimate of the measurement error (Parrent et al. 2012). The reduced $\chi^2$ around the best fit explosion time is about 1.2 (there are 17 degrees of freedom). In Figure 1 we consider three different velocity power-law indices

[4] Interestingly, this indicates that these different features are due to different line opacities within a flow with the same velocity power-law profile and are not separate velocity components in the ejecta. This argues against situations where the high-velocity features are generated by a separate event during or prior to the explosion (e.g., Piro 2011).

[5] Other absorption features are measured, but we restrict our study to these three since they are some of the most widely available in SN Ia literature.

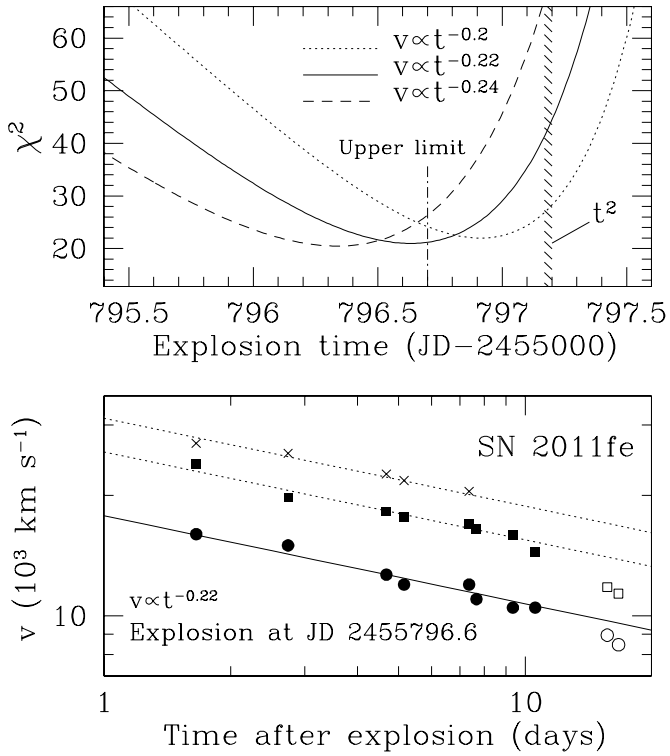


**Figure 1.** Top panel plots the $\chi^2$ found by fitting the velocity evolution as a power law with time for different explosion times and various power-law indices as labeled. We draw a vertical dot-dashed line at the time of an upper limit from a non-detection and a shaded region at the explosion time inferred by fitting a $t^2$ rise (Nugent et al. 2011). In the bottom panel we plot the observed low-velocity Si II λ6355 (circles), high-velocity Si II λ6355 (squares), and high-velocity Ca II H and K (crosses). Filled and open symbols indicate data that was used or not used for the fit, respectively. The lines show our best fit velocity evolution for $v \propto t^{-0.22}$, and the solid line indicates the $v_{\rm ph}$ we use in subsequent analysis.

centered around the model prediction of $v \propto t^{-0.22}$. This shows that the model provides a good description of the data, and that assuming that the power-law index is known, the explosion time is measured to within about ±0.25 day. However, assuming slightly different power laws produces fits with similar quality and results in explosion times that vary by about ≈1 day. Since theoretically $v \propto t^{-0.22}$ is the preferred velocity profile we consider JD2455796.6 to be the most likely explosion time with an uncertainty of roughly ±0.5 day. This is actually very similar (within 0.1 day) to the non-detection by Nugent et al. (2011). In the bottom panel we present the velocity data along with our best fit velocity evolutions. Open symbols indicate data that were not used for the fit because they are near peak where the velocity profile is not expected to be a power law.

For any given explosion time we can look for the $^{56}$Ni distribution that produces the observed luminosity. The fitting is done via a $\chi^2$ minimization over $\beta$ and $x_{1/2}$ in the parameterization of $X_{56}$ given by Equation (11). Assuming a ≈10% error in the bolometric luminosity measurements, the $\chi^2$ per degree of freedom of the best fit $^{56}$Ni distribution is less than two. Contours of constant $\chi^2$ are plotted in Figure 2 to demonstrate the quality of the fit and how much degeneracy there is. Although this does not prove that the $^{56}$Ni distribution we derive is unique, it at least shows that it does a good job of modeling the data. The results from fitting the photometric observations are presented in Figure 3. In this particular case we use the time of the non-detection for the explosion time, which is sufficiently close to our preferred time so that the qualitative features

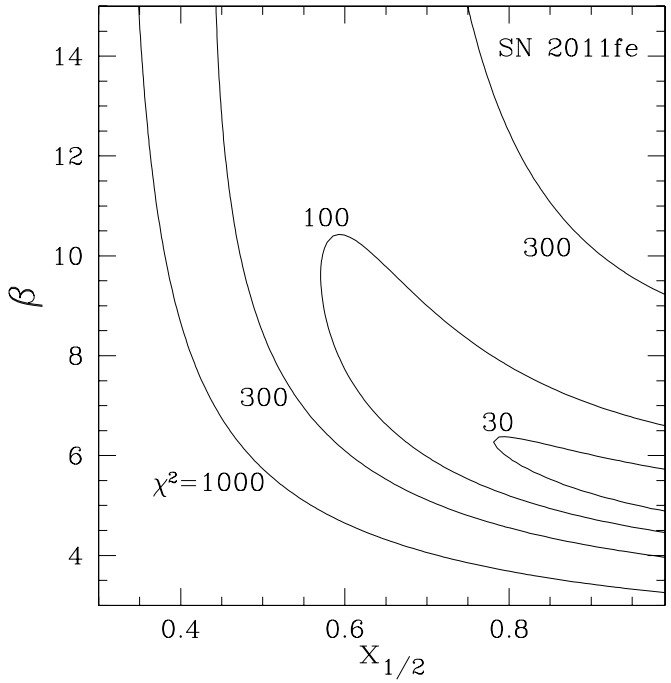


**Figure 2.** Contours of constant $\chi^2$ (as labeled) from fitting for the $^{56}$Ni distribution (through $\beta$ and $x_{1/2}$) needed to explain the rising light curve of SN 2011fe. This demonstrates that a relatively low value of $\beta$ is needed, which in turn implies a shallow distribution of $^{56}$Ni. Although not presented in this paper, the fits for SNe 2009ig and 2012cg are similar.

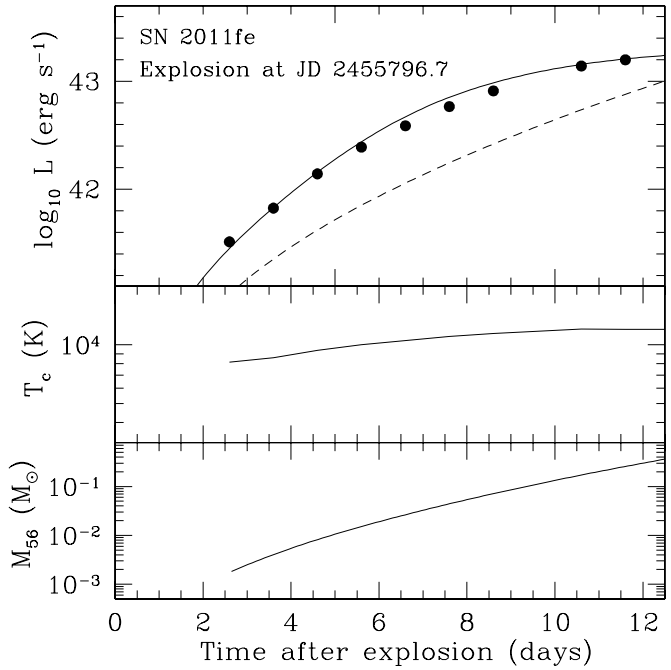


**Figure 3.** Summary of the fits to SN 2011fe. The top panel shows the inferred bolometric luminosity (filled circles), the fit bolometric luminosity (solid curve), and the local heating from $^{56}$Ni of $L_{56}$ (dashed curve) given by Equation (8). The middle panel shows the color temperature, and the bottom panel shows $M_{56} = L_{56}/\epsilon$.

are unchanged. In the top panel we compare the inferred bolometric light curve (filled circles) to the model fit (solid curve). We also plot the contributions from local heating $L_{56}$ (dashed curve) to show how well the bolometric luminosity reflects the underlying $^{56}$Ni distribution. We find a range of $L_{56}/L \sim$ 0.2–0.6, and typically $L_{56}/L \sim 0.3$, during the early times

of the SNe. This means that although the match is not exact, the underlying $^{56}$Ni distribution is roughly represented by the observed luminosity and nonlocal effects are not dominating. Therefore $^{56}$Ni must be present, at least in some amount, at the depths that are probed by the earliest emission. To test the robustness of this conclusion, we varied the $^{56}$Ni distribution (by varying $\beta$ and $x_{1/2}$) by two standard deviations from the best fit values. We still found that $^{56}$Ni must be present near the exploding star's surface, showing that it is difficult to explain the early rise without some $^{56}$Ni at the diffusion depth.

The middle panel of Figure 3 shows the inferred color temperature $T_c$. This confirms our earlier discussion of the opacities in Section 2, and that the temperature at the diffusion depth (which is greater than $T_c$ by a factor of $\approx \tau^{1/4}$, where $\tau \approx 30$ is the optical depth at the diffusion depth) is always sufficiently high that carbon and oxygen will not be fully recombined.

The bottom panel shows the mass of $^{56}$Ni above the diffusion wave depth, given by

$$M_{56}(t) = L_{56}(t)/\epsilon(t). \quad (14)$$

This is roughly independent of the explosion time because it is just set by the bolometric luminosity at any given time. In contrast, $T_c$ changes with explosion time because an explosion further in the past implies more expansion at any given time and thus a smaller $T_c$. This means that an additional constraint on the explosion time could be made via a temperature measurement, although this requires detailed spectral modeling that is outside the scope of this work (see the discussion of $t_{\rm min}$ in Piro & Nakar 2013).

### 3.2. Radius Constraints and Shallowest $^{56}$Ni for SN 2011fe

Using the data from Nugent et al. (2011) and a non-detection $\approx$7 hr earlier, Bloom et al. (2012) argued that the progenitor of SN 2011fe had a radius $\lesssim 0.02\,R_\odot$ by using models of shock-heated cooling (Piro et al. 2010; Rabinak et al. 2012). But this assumed that the time of explosion could be accurately determined from extrapolating $t^2$ back in time. As emphasized in Piro & Nakar (2013), this is not generally a robust method for finding the explosion time (see also Section 4), so it is worth revisiting the radius constraint for a range of explosion times.

In Figure 4 we plot the early data and non-detection upper limit for SN 2011fe for two different explosion times. The theoretical curves include radioactive heating (dashed curves) and shock-heated cooling (solid curves). The first thing to note is that $^{56}$Ni cannot always be present at the earliest times and still produce the observed light curves. In the bottom panel we had to cut off the $^{56}$Ni for times earlier than 0.9 day after explosion in order to not overpredict the $g$-band upper limit reported in Bloom et al. (2012). (In the top panel no $^{56}$Ni cut-off is needed.) This implies that for earlier explosion times there is a sharp cut-off in the $^{56}$Ni distribution near the depth that generates the luminosity of the first detected light. This is not unexpected since $^{56}$Ni probably does not extend to the very surface and the earliest emission will be due to the diffusive tail. In Section 3.5 we further discuss what depth in the WD is implied by this time.

The other thing to note from Figure 4 is that when the explosion time is further in the past, upper limits on the emission from shock-heated cooling (solid curves) are not as stringent. Using the models from Piro et al. (2010) we find that when the explosion is merely 0.5 day further in the past (the bottom panel) the radius can be a factor of 1.9 greater than in the top panel.

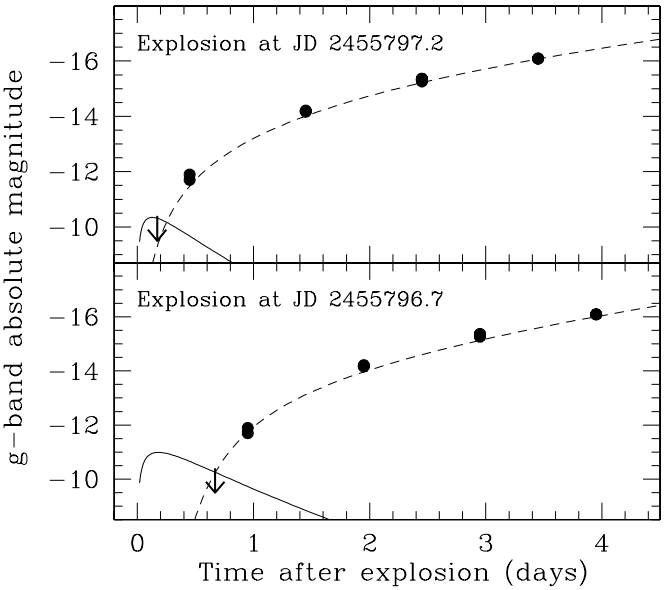


**Figure 4.** Comparison of the early $g$-band data (Nugent et al. 2011) and a non-detection upper limit (Bloom et al. 2012) to theoretical light curves from radioactive heating (dashed curves) and shock-heated cooling (solid curves) calculated according to Piro et al. (2010). This does not include the suppression of the shock-heated cooling (or "drop out") that occurs when the diffusion wave moves into ideal gas dominated material (Rabinak et al. 2012). The top panel is roughly the explosion time inferred from a $t^2$ extrapolation. The bottom panel assumes that the explosion occurred 0.5 day earlier, for which the radius constraint is a factor of 1.9 larger.

Another potentially important effect that is not included in Figure 4 is the "drop out" in the shock-heated cooling emission that is expected once the diffusion wave exposes the depth where the shock is matter rather than radiation dominated. This is expected to occur $\sim$ hours after explosion for a typical WD radius (Rabinak et al. 2012). Although we do not consider explosion times earlier than the non-detection of Nugent et al. (2011) in Figure 4, it is possible that the explosion occurred before ($\sim$0.5 day) this time, and the non-detection is simply during the dark phase between the drop out and the latter $^{56}$Ni heating. Bloom et al. (2012) find that the drop out limits the radius constraint posed by their upper limit. If the explosion is 1 day before the date estimated by Nugent et al. (2011), then the uncertainty in the limit on the radius of the progenitor of SN 2010fe is somewhat increased. Hence the progenitor can be as large as $\sim 0.1\,R_\odot$.

### 3.3. SN 2012cg

The velocities and photometry for SN 2012cg are summarized in Silverman et al. (2012). Further photometry is presented by Munari et al. (2013), including data around the peak identified to occur at roughly JD2456083.0. The velocity fitting results are shown Figure 5 (again taking $\Delta v = 500$ km s$^{-1}$). The best fit explosion time is JD2456063.5, but the strength of the fit is not as strong as for SN 2011fe. In comparison, using $t^2$ Silverman et al. (2012) find JD2456063.2 $\pm$ 0.2 (the shaded region in the top panel of Figure 5), which is marginally consistent with our fits. The light curve modeling from the observed $B$, $V$, and $R$ measurements use a distance modulus of 30.9. The summary of our results from the photometric data are presented in Figure 6.

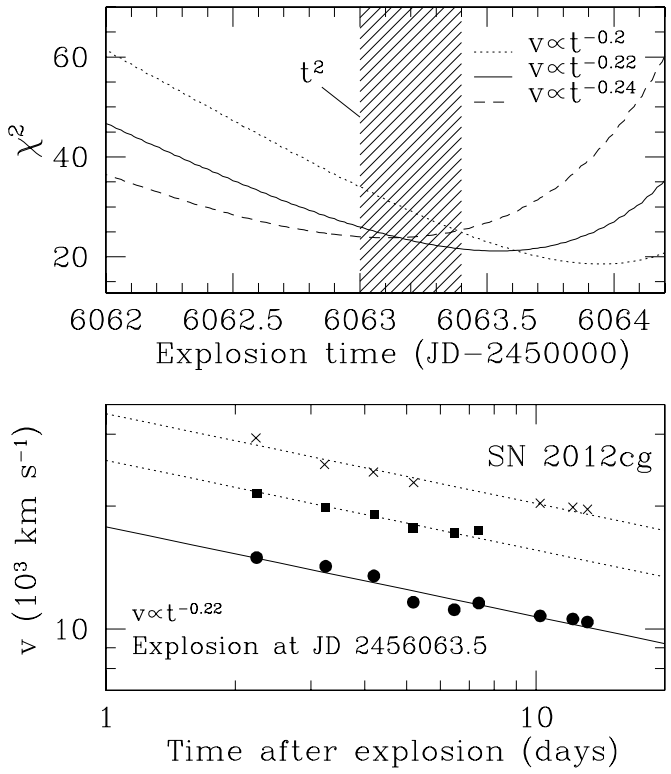


**Figure 5.** Same as Figure 1, but for SN 2012cg. The shaded region shows the inferred explosion time from Silverman et al. (2012) using $t^2$.

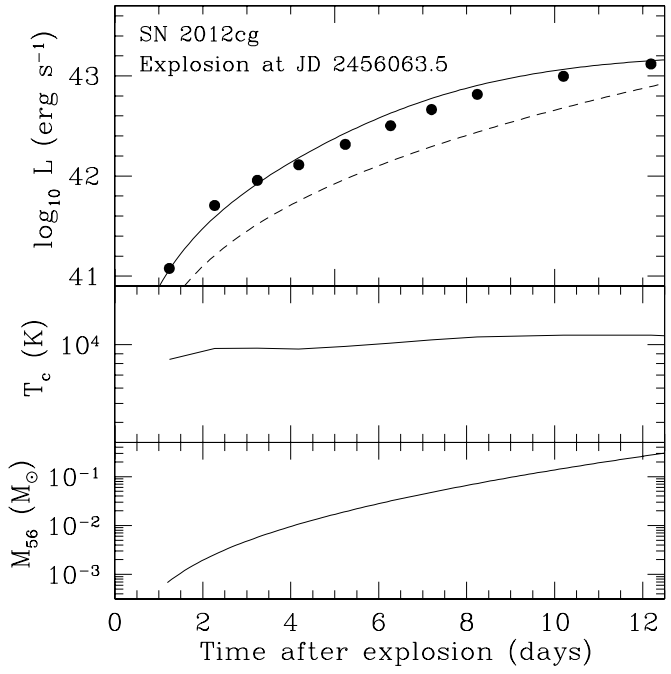


**Figure 6.** Same as Figure 3, but for SN 2012cg.

### 3.4. SN 2009ig

The velocities and photometry for SN 2009ig are presented in Foley et al. (2012). The time of $B$-band peak is at JD2455080.54, and the distance modulus is 32.6. The evolution of the Si II λ6355 absorption feature is a little more complicated in this case and deserves some discussion. At early times (earlier than 12 days before $B$-band peak), Si II appears to only have a high velocity component, and a low-velocity component grows to be more prominent later. We take the low-velocity component as indicative of the photosphere, but use both the high- and low-velocity components when fitting the $v \propto t^{-0.22}$ power law. Data taken when the features overlap could potentially bias the fit due to blending, but we did not find that it has an adverse impact on our fits.

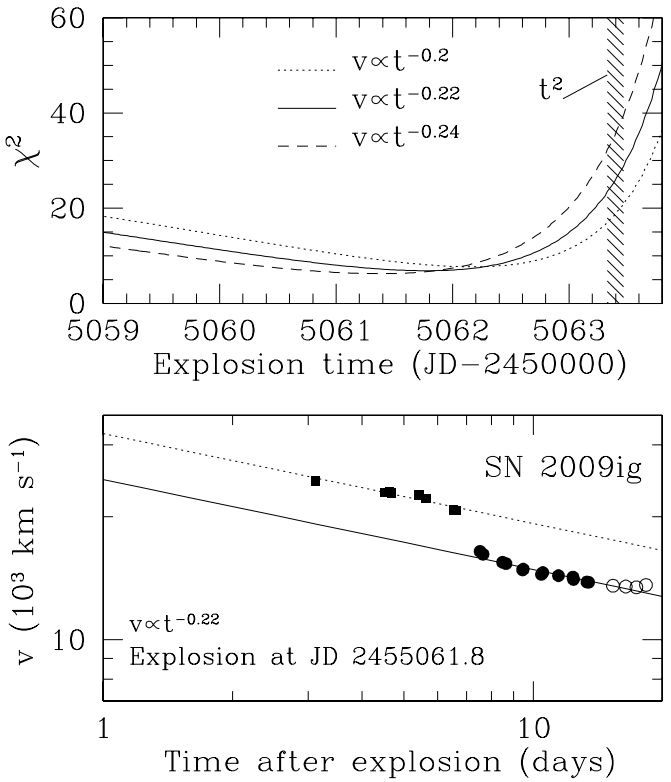


**Figure 7.** Same as Figure 1, but for SN 2009ig. Open circles indicate data that was not used for the fit because they are too close to peak. Although an explosion time of JD2455061.8 is favored, the constraints are not as strong as for the other SNe.

In Figure 7 we summarize the velocity fitting. Only high- and low-velocity Si II are used in this case. High-velocity Ca II H and K absorption features may be blended with Si II λ4130, and are not presented by Foley et al. (2012). The best fit time of explosion is at JD2455061.8. In comparison, using a $t^2$ rise Foley et al. (2012) infer an explosion time JD2455063.4 ± 0.07. Although SN 2009ig has the least constraining fits of any of the SNe, this later explosion time seems difficult to reconcile with the velocity evolution unless $v(t)$ is a much shallower power law with time than that expected from theory. In Figure 8 we plot the best fit light curve properties as was done for the other SNe.

### 3.5. Comparing and Contrasting Events

In Figure 9 we plot the distributions of $^{56}$Ni inferred for the three SNe Ia modeled above. In each case multiple values for the explosion time are considered to demonstrate how inferences on $X_{56}$ change with this parameter. The solid lines in each panel indicate the preferred explosion time. For SN 2011fe (top panel), thick lines show the distribution covered by the photometric observations of Vinkó et al. (2012) and thin lines show the distribution inferred by the earlier observations by Nugent et al. (2011). This shows that since $\Delta M_{\rm diff} \propto t^{1.76}$, having observations just a day or two earlier can probe much shallower regions of the ejecta. For the preferred explosion time,

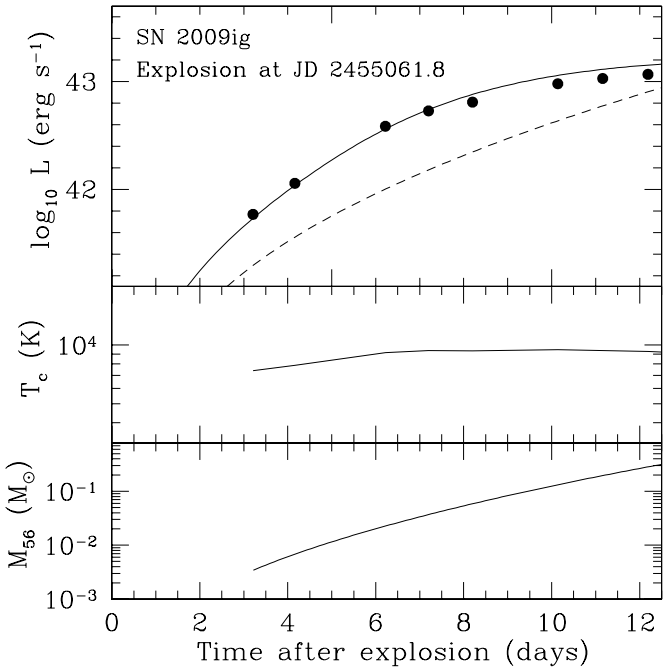


**Figure 8.** Same as Figure 3, but for SN 2009ig.

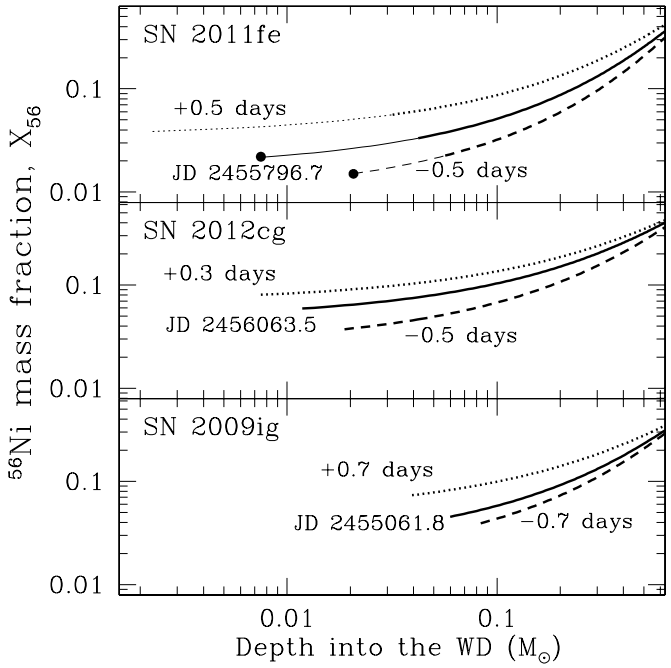


**Figure 9.** Inferred distribution of $^{56}$Ni as a function of depth in the WD. In each case we compare multiple explosion times, with the solid lines indicating the value preferred by fitting $v \propto t^{-0.22}$. The depth into the star is assumed to scale as $\Delta M_{\rm diff} \propto t^{1.76}$ with a normalization of $\Delta M_{\rm diff} = 1.4\ M_\odot$ at light curve peak. For SN 2011fe (top panel), the thick curves correspond to the constraints from the observations by Vinkó et al. (2012), and the thin curves correspond to the observations by Nugent et al. (2011). The filled circles indicate the shallowest allowed deposits of $^{56}$Ni so as not to overshoot the upper limit presented by Bloom et al. (2012).

$X_{56} \approx 2 \times 10^{-2}$ at a depth of $\Delta M_{\rm diff} \approx 10^{-2}\ M_\odot$. These results are roughly consistent with models presented by Piro (2012), which assumed a similar explosion time but did not include the diffusive tail. As discussed in Section 3.2, the upper limit on the luminosity at early times implies that there must be a cut-off in the $^{56}$Ni distribution for some explosion times. These shallowest $^{56}$Ni depths are indicated by filled circles in the top panel of Figure 9 (although not mentioned in Section 3.2, for the −0.5 day curve, $^{56}$Ni cannot be shallower than the depth of the diffusion wave at 1.7 days after the explosion).

The $^{56}$Ni distributions in SN 2012cg and SN 2009ig are fairly similar to SN 2011fe over similar depths. The main difference is that SN 2012cg shows somewhat more $^{56}$Ni around a range of $\Delta M_{\rm diff} \approx 10^{-2}$–$10^{-1}\ M_\odot$. Does this imply that SN 2012cg has more shallow burning products? Analysis of the spectra indicates that SN 2011fe has considerably more unburned carbon at shallow depths than SN 2012cg (Parrent et al. 2012), which is at least consistent with this hypothesis.

SN 2009ig also has a number of differences that are worth discussing. The Si II velocities at ≈10 days past explosion are considerably higher in this event than either SN 2011fe or SN 2012cg. If this indicates a difference in the actual explosion energy, then using $v_{\rm ph} \propto E^{0.39}$ (Piro & Nakar 2013) argues that SN 2009ig was a factor of ≈2 more energetic than the other two events. Such an explanation seems difficult to reconcile with the peak luminosity of SN 2009ig, which is fairly standard for SNe Ia. Another attractive possibility is that the large velocities are due to an asymmetric explosion that is directed more toward the observer (Maeda et al. 2010a). For such larger velocities, there is more expansion and a generally cooler SN, as can be seen by the $T_c$ presented in the middle panel of Figure 8. Foley et al. (2012) note that SN 2009ig is considerably redder in the UV at early times in comparison to other SNe Ia and typical templates. Is this just due to the larger velocities? Another possibility is that these colors are due to iron-peak elements near the surface, which again would be consistent with an explosion directed toward the observer. The mass fraction of $^{56}$Ni for SN 2009ig is fairly similar to the other SNe at a depth of ≈0.1 $M_\odot$, and data is not available early enough to probe shallower regions.

Although the many differences found for SN 2009ig are tantalizing, we emphasize that these conclusions all hinge on our assumption that roughly $v \propto t^{-0.22}$. If for some reason the velocity profile of SN 2009ig is different than the other two SNe, then these conclusions must be revised. On the other hand, if the velocity profile *is* significantly different in this case, that might be interesting in and of itself. If the SN is asymmetric, it also limits the applicability of our models, which assume spherical symmetry, in assessing the properties of this event. Properties we infer, such as the $^{56}$Ni distribution, maybe then reflect some sort of angle-averaged property of the ejecta rather than directly measuring the ejecta profiles. Future numerical work should explore how well the correlations we discuss (between velocity, temperature, and so on) still hold for asymmetric explosions, and as a function of viewing angle.

### 3.6. Progenitor Models

For all three SNe we study, $^{56}$Ni must be present at least ≈ 0.1 $M_\odot$ from the WD surface, and as shallow as ≈$10^{-2}$ $M_\odot$ from the surface for SN 2011fe and SN 2012cg (see Figure 9). It is therefore worth discussing the implications for progenitor models and the character of the explosive burning.

As a comparison, Hachinger et al. (2013) performed detailed UV/optical spectral modeling of SN 2010jn. From this analysis they also infer iron-group elements near the surface. DDT models can produce $^{56}$Ni near the WD surface (e.g., Iwamoto et al. 1999), but to get radioactive material as shallow as ≈$10^{-2}$ $M_\odot$ may require a strongly mixed, off-center deflagration (Maeda et al. 2010b). In DDT models with many ignition points

that have fairly stratified ashes, radioactive elements are not present near the surface. A gravitationally confined detonation also produces iron-peak elements near the surface when a bubble rises and breaks (Meakin et al. 2009).

Another interesting scenario that may produce shallow radioactive heating is the explosive ignition of a helium shell in a double-detonation. The depth and amount of $^{56}$Ni we infer is not dissimilar to the helium shell masses needed for detonation and the total amount of radioactive material found for such events (Shen & Bildsten 2009; Fink et al. 2010). The main problem with such models is that if iron-peak elements are too abundant, they tend to produce colors that are too red and spectra that are inconsistent with normal SNe Ia (Kromer et al. 2010; Sim et al. 2012). But if the helium burns in a lateral detonation which does not process the fuel as completely to iron-peak elements (Townsley et al. 2012), this may overcome some of the difficulties double-detonation models have in reproducing observed SNe Ia.

## 4. IS A $t^2$ RISE SPECIAL?

A common practice with recent SN Ia observations is to determine the time of explosion by fitting the rising luminosity (often in a single band) with a $t^2$ curve (Nugent et al. 2011; Milne & Brown 2012; Foley et al. 2012; Silverman et al. 2012). Studies of composite light curves formed from stacking many SNe, which allow the power-law index to vary, find power-law indices of $1.8 \pm 0.2$ (Conley et al. 2006), $1.8^{+0.23}_{-0.18}$ (Hayden et al. 2010), and $2.20^{+0.27}_{-0.19}$ (Ganeshalingam et al. 2011). This then begs the question, is $t^2$ (or any other power law) fundamental, and if not, what is the origin of these results?

Our discussion in Section 2 shows that a priori a power-law luminosity rise is not generally expected. The luminosity is driven by a combination of two factors: (1) the diffusion wave propagation, $\Delta M_{\rm diff}(t)$, and (2) the distribution of $^{56}$Ni fraction, $X_{56}$. The exposed mass does indeed evolve as a power law, with (Piro 2012)

$$\Delta M_{\rm diff}(t) \propto t^{2(1+1/n)/(1+1/n+\beta)}, \quad (15)$$

where $n$ is the polytropic index and $\beta$ is the power-law index of the velocity gradient. For $n = 3$ and $\beta = 0.186$ (Sakurai 1960), this results in $\Delta M_{\rm diff} \propto t^{1.76}$ (as in Equation (1)). In contrast, the $^{56}$Ni distribution is not well constrained by theory and may, in principle, vary in many ways. A power-law rise of the bolometric luminosity is expected only if the $^{56}$Ni fraction evolves as a power law as well, namely $X_{56} \propto t^{\alpha}$. In this case the bolometric luminosity evolves as $L \propto t^{1.76+\alpha}$ and since the photospheric radius is roughly $\propto t^{0.78}$ (Piro & Nakar 2013), the observed temperature evolves roughly as $T_c \propto t^{(0.2+\alpha)/4}$. This result was obtained by Piro (2012) when the diffusive tail was not included, and we find that it still holds with the more detailed analysis presented in Section 2. Since we do not expect $X_{56} \propto t^{0.24}$, our conclusion is that a $t^2$ rise (bolometric or in a single band) is probably not a generic property of SNe Ia. We also do not expect the rise to follow exactly any other power law. Moreover, since most explosion models predict a sharp decrease of $X_{56}$ in the outermost layers of the ejecta, the light curve is expected to rise exponentially (due to diffusive tail contribution) at very early times. How early this exponential phase take place depends on the depth of the shallowest $^{56}$Ni deposit.

What is then the explanation of the fact that analysis of large SNe samples are found to be consistent with a power-law rise with indices in the range ≈1.8–2.2? It is probably a combination

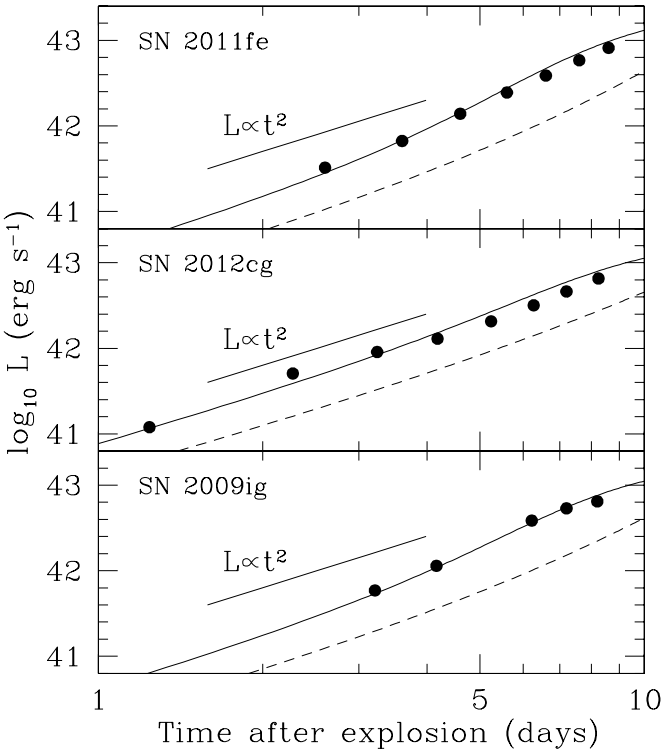


**Figure 10.** Bolometric light curves for each of the three SNe (from the top panels of Figures 3, 6, and 8), but in this case plotted with logarithmic axes to emphasize power-law behavior. Again the dashed lines are $L_{56}$.

of two things. First, the unknown explosion time enables a reasonable fit even if the light curve is not exactly a power law. Second, in the depth range explored by most of these SNe rising phases, the $X_{56}$ is not varying by a large amount. This is because the first observation of most SNe Ia takes place only a few days to a week after the explosion, so that the $^{56}$Ni is distributed roughly uniformly or slowly increasing with depth.

In Figure 10, we plot the bolometric light curves and fits for the three SNe we have been studying on a logarithmic scale to emphasize power-law dependencies. This shows that the light curves are not rising exactly as power laws, but that power law fits can provide a reasonable description of the data (although for SNe 2001fe the rise is found to be slightly faster than $t^2$). This is because in all three of these SNe the $X_{56}$ is rising rather gradually over the depth range probed by the observations.

There have been some attempts to explain why there should be a $t^2$ rise, but none of these provide arguments that are expected to hold in detail. The most simplified explanation is a fixed color temperature with a radius that increases linearly with time (Riess et al. 1999). This model does not explain why the temperature should be constant, and more importantly, in real SNe the color temperature does typically vary with time. A more fundamental explanation for a $t^2$ rise is given by Arnett (1982), which considers radioactive heating with thermal diffusion (also see the Supplementary Information of Nugent et al. 2011). This model makes two explicit approximations: (1) it ignores the velocity gradient, obtaining $\Delta M_{\rm diff} \propto t^2$ (basically setting $\beta = 0$ in Equation (15)), and (2) it assumes that $X_{56}$ is constant. Together these factors result in a $t^2$ rise, but only for assumptions that are not realistic.

To conclude, we expect the early rise to depend on the particular physical conditions in any given event and thus to possibly vary from one SN to another. It will be important to

test this hypothesis in the future by building bolometric light curves from observations to infer just how much diversity there really is. Detailed numerical calculations of the rise will also be useful for understanding how much the early luminosity can change depending on composition and radiative transfer effects. Whatever the results are, extrapolating a light curve back in time with $t^2$ is not a reliable method for inferring the explosion time.

## 5. CONCLUSIONS AND DISCUSSION

Using early observations of three SNe Ia, and assuming that the absorption feature velocities evolve as $v \propto t^{-0.22}$, we constrained the explosion times and shallow distributions of $^{56}$Ni. We then used these findings to revisit the radius constraints on the progenitor of SN 2011fe (in Section 3.2), and discuss the $t^2$ rise that is reported for many SNe Ia (in Section 4). Using such methods, we are only able to constrain the time of explosion to roughly $\pm 0.5$ day and the corresponding $^{56}$Ni mass fraction at a given depth to within a factor of roughly $\pm 3$. Nevertheless, it is difficult to avoid the fact that $^{56}$Ni must be present at relatively shallow depths ($\sim 10^{-2}\ M_\odot$ from the WD surface), even if in very small amounts ($X_{56} \sim 10^{-2}$).

SN 2011fe and SN 2012cg appear very similar in most respects, including the rise time, $^{56}$Ni distribution, and energetics. The main difference is that SN 2012cg has a slightly larger amount of shallow $^{56}$Ni. SN 2009ig is somewhat different than the other two SNe. Although its $^{56}$Ni distribution over the same depths probed in SN 2011fe and SN 2012cg is fairly similar, it has higher velocities at any given time and its best fit time of explosion has the largest discrepancy with previous estimates ($\approx$1.6 days earlier). This is curious because the peak luminosity of SN 2009ig is fairly normal in comparison to the other SNe, and thus the amount of $^{56}$Ni and the energetics should be similar. One possible solution is if SN 2009ig is asymmetric with higher velocities directed toward the observer (Maeda et al. 2010a). Unfortunately our results on SN 2009ig are somewhat tentative because it has the least constrained time of explosion. This is because the low velocity Si II is only seen relatively late, and thus has a rather flat evolution with time. Hopefully our work inspires more detailed modeling of SN 2009ig in the future to test our conclusions.

These comparisons show how important it is to have the earliest observations possible. Out of the events we consider, SN 2011fe is the best constrained because it shows the largest velocity gradients. Just a few velocity measurements very early in the light curve can be more helpful in determining the explosion time than having many measurements at later times. Furthermore, since $\Delta M_{\rm diff} \propto t^{1.76}$, having observations only a day or two earlier probe much shallower depths in the ejecta. Although not discussed much here, having one or two early spectra that can be used for modeling the surface temperature can also provide tight constraints on the explosion time (Piro & Nakar 2013).

With just these three events, we are already beginning to see correlations between the various features that determine the early light curve rise. In the future, studies should look for connections between the early rise and a larger range of properties, such as the late nebular features or the characteristics of the host galaxies. It will also be useful to compare spectral modeling methods for measuring surface abundances (like in Hachinger et al. 2013) with the techniques we present here. If used together, they may be more constraining on the nature of the progenitors and the details of the explosive burning. Finally, it would worth exploring the early light curves of non-standard SNe Ia, like SN 2002cx (Li et al. 2003; Foley et al. 2013). Such studies will be important for fully utilizing the observations available in this new era of early detections of exploding WDs.

We thank Ryan Foley, Mohan Ganeshalingam, and Jeffrey Silverman for assistance with assessing data and discussing observations. We also thank Federica Bianco, Ryan Chornock, Luc Dessart, Stephan Hachinger, Keiichi Maeda, Peter Nugent, and Re'em Sari for helpful discussions or comments on previous drafts. A.L.P. was supported through NSF grants AST-1212170, PHY-1151197, and PHY-1068881, NASA ATP grant NNX11AC37G, and by the Sherman Fairchild Foundation. E.N. was partially supported by an ERC starting grant (GRB-SN 279369) and by the I-CORE Program of the Planning and Budgeting Committee and the ISF (1829/12).

## REFERENCES

Arnett, W. D. 1982, ApJ, 253, 785
Bloom, J. S., Kasen, D., Shen, K. J., et al. 2012, ApJL, 744, L17
Conley, A., Howell, D. A., Howes, A., et al. 2006, AJ, 132, 1707
Fink, M., Röpke, F. K., Hillebrandt, W., et al. 2010, A&A, 514, A53
Foley, R. J., Challis, P. J., Chornock, R., et al. 2013, ApJ, 767, 57
Foley, R. J., Challis, P. J., Filippenko, A. V., et al. 2012, ApJ, 744, 38
Ganeshalingam, M., Li, W., & Filippenko, A. V. 2011, MNRAS, 416, 2607
Hachinger, S., Mazzali, P. A., Sullivan, M., et al. 2013, MNRAS, 429, 2228
Hayden, B. T., Garnavich, P. M., Kessler, R., et al. 2010, ApJ, 712, 350
Hillebrandt, W., & Niemeyer, J. C. 2000, ARA&A, 38, 191
Hoyle, F., & Fowler, W. A. 1960, ApJ, 132, 565
Iben, I., Jr., & Tutukov, A. V. 1984, ApJS, 54, 335
Iwamoto, K., Brachwitz, F., Nomoto, K., et al. 1999, ApJS, 125, 439
Khokhlov, A. M. 1991, A&A, 245, 114
Kromer, M., Sim, S. A., Fink, M., et al. 2010, ApJ, 719, 1067
Li, W., Filippenko, A. V., Chornock, R., et al. 2003, PASP, 115, 453
Livne, E., & Arnett, D. 1995, ApJ, 452, 62
Maeda, K., Benetti, S., Stritzinger, M., et al. 2010a, Natur, 466, 82
Maeda, K., Röpke, F. K., Fink, M., et al. 2010b, ApJ, 712, 624
Meakin, C. A., Seitenzahl, I., Townsley, D., et al. 2009, ApJ, 693, 1188
Milne, P. A., & Brown, P. J. 2012, arXiv:1201.1279
Munari, U., Henden, A., Belligoli, R., et al. 2013, NewA, 20, 30
Nakar, E., & Sari, R. 2010, ApJ, 725, 904
Nakar, E., & Sari, R. 2012, ApJ, 747, 88
Nomoto, K., Sugimoto, D., & Neo, S. 1976, Ap&SS, 39, L37
Nomoto, K., Thielemann, F.-K., & Yokoi, K. 1984, ApJ, 286, 644
Nugent, P. E., Sullivan, M., Cenko, S. B., et al. 2011, Natur, 480, 344
Parrent, J. T., Howell, D. A., Friesen, B., et al. 2012, ApJL, 752, L26
Patat, F., Cordiner, M. A., Cox, N. L. J., et al. 2013, A&A, 549, A62
Perlmutter, S., Aldering, G., Goldhaber, G., et al. 1999, ApJ, 517, 565
Pinto, P. A., & Eastman, R. G. 2000, ApJ, 530, 757
Piro, A. L. 2011, ApJL, 738, L5
Piro, A. L. 2012, ApJ, 759, 83
Piro, A. L., Chang, P., & Weinberg, N. N. 2010, ApJ, 708, 598
Piro, A. L., & Nakar, E. 2013, ApJ, 769, 67
Rabinak, I., Livne, E., & Waxman, E. 2012, ApJ, 757, 35
Richmond, M. W., & Smith, H. A. 2012, JAVSO, 40, 872
Riess, A. G., Filippenko, A. V., Challis, P., et al. 1998, AJ, 116, 1009
Riess, A. G., Filippenko, A. V., Li, W., et al. 1999, AJ, 118, 2675
Sakurai, A. 1960, CPAM, 13, 353
Shappee, B. J., & Stanek, K. Z. 2011, ApJ, 733, 124
Shen, K. J., & Bildsten, L. 2009, ApJ, 699, 1365
Silverman, J. M., Ganeshalingam, M., Cenko, S. B., et al. 2012, ApJL, 756, L7
Sim, S. A., Fink, M., Kromer, M., et al. 2012, MNRAS, 420, 3003
Tanaka, M., Mazzali, P. A., Benetti, S., et al. 2008, ApJ, 677, 448
Townsley, D. M., Moore, K., & Bildsten, L. 2012, ApJ, 755, 4
Vinkó, J., Sárneczky, K., Takáts, K., et al. 2012, A&A, 546, A12
Webbink, R. F. 1984, ApJ, 277, 355
Whelan, J., & Iben, I., Jr. 1973, ApJ, 186, 1007
Woosley, S. E., & Weaver, T. A. 1994a, ApJ, 423, 371
Woosley, S. E., & Weaver, T. A. 1994b, in Les Houches Session LIV, Supernovae, ed. S. Bludman, R. Mochovitch, & J. Zinn-Justin (Amsterdam: North Holland), 63